The production and diffusion of vorticity in duct flow

By E. BRUNDRETT AND W. D. BAINES
Department of Mechanical Engineering University of Toronto, Toronto

(Received 14 June 1963 and in revised form 2 December 1963)

Secondary flows in non-circular ducts are accompanied by a longitudinal component of vorticity. The equation of motion defining this component in a turbulent flow is composed of three terms giving the rates of production, diffusion and convection. Since the expression for production is the second derivative of Reynolds stress components, longitudinal vorticity cannot exist in laminar flow. For turbulent flow in a square duct the Reynolds stress tensor is examined in detail. Symmetry requirements alone provide relationships showing that the production is zero along all lines of symmetry. General characteristics of flow in circular pipes are sufficient to indicate where the production must be greatest. Experimental measurements verify this result and define the point density of production, diffusion and convection of vorticity. Data also indicate that the basic pattern of secondary flow is independent of Reynolds number, but that with increasing values of Reynolds number the flows penetrate the corners and approach the walls. A similar experimental investigation of a rectangular duct shows that the corner bisectors separate independent secondary flow circulation zones. Production of vorticity is again associated with the region near the bisector. However, there is some evidence that the secondary flow pattern is not so complex as inferred from the distortion of the main longitudinal flow.

1. Introduction

There is ample evidence that turbulent flow in a long duct of non-circular cross-section is accompanied by lateral spiral motions. This secondary flow convects main flow momentum and energy towards the wall in some regions and away from the wall in other regions. Thus, mean flow streamlines must be helical and not the straight lines found in circular pipes. Nikuradse (1926) was probably the first to delineate the discrepancies between flow in circular pipes and square ducts. Lines of constant velocity or isovels are displaced towards the corners and away from the mid-point of the walls compared to the isovels for laminar flow (figure 1). Prandtl (1927) suggested that these were the result of secondary flows toward the corners which to satisfy continuity required a return flow at the mid-point of the walls. It was also postulated that these were the result of the turbulent fluctuations along the isovels giving a net flow normal to the isovel wherever a variation in curvature occurred. The magnitude of the secondary velocities could not be measured at that time because of the error introduced by the presence of the yaw-meter when used in regions possessing mean velocity gradients.

As a result of the development of the hot-wire anemometer these velocities can now be measured and are found to be smaller than the root-mean-square turbulent velocity. Hoagland (1960) found that the flow pattern was exactly that predicted by Prandtl but did not pursue the study of the origins. Other recent studies have been focused on the primary flow. Leutheusser (1963) has found that in square and rectangular ducts the inner law provides a good description of flow in the neighbourhood of the wall but in the centre of the duct the velocity distribution does not follow the outer-law formulation. Thus con-

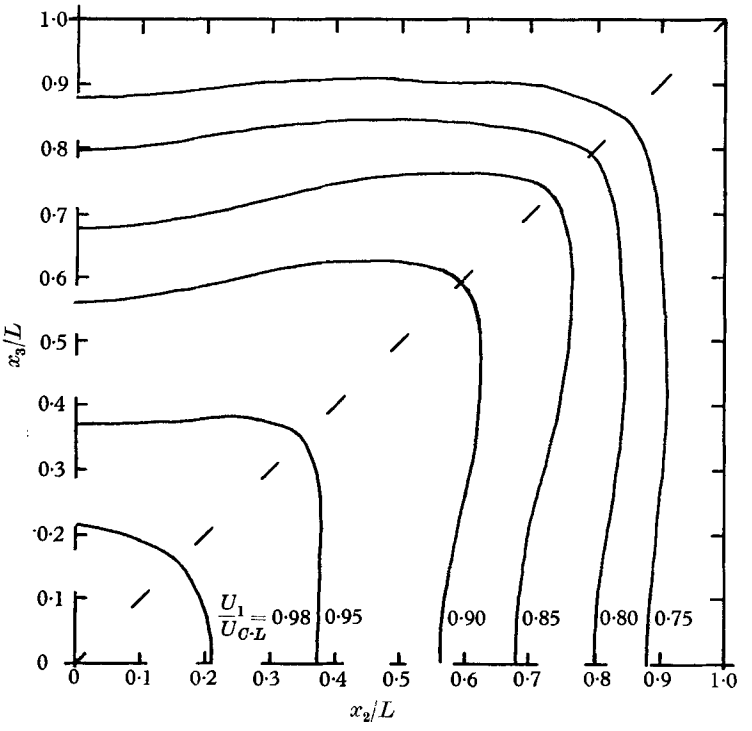

FIGURE 1. Isovels of axial velocity for flow in a square duct (Leutheusser 1963). L = 1·5 in., $U_{C\cdot L}$ = 65·9 ft./sec, U_{av} = 54·8 ft./sec, $U_{av}D_e/\nu$ = 83,000.

temporary engineering practice for the prediction of heat transfer and shear distribution in complex-shaped passages is in error because of the assumption of an inner-law velocity distribution over the entire cross-section. Even more serious is the neglect of the secondary flows which tend to produce uniform shear and heat transfer around the periphery of the duct. However, in a currently used approximation in hydraulics the transport coefficients are considered uniform which would be the result of the secondary currents being very large.

In this paper the origin and dissipation of the secondary flows in a square duct are discussed, and experimental evidence is introduced showing the mechanism by which these arise and are controlled. The commonly used momentum and energy equations are not significant in this description because the secondary velocities play only the role of convecting mechanisms. The analysis is based entirely on the equation for mean-flow longitudinal vorticity. The fluid

elements must possess an angular velocity about an axis in the main flow direction if the secondary velocities exist. The essential information as to where the secondary flows originate and are dissipated is obtained from a detailed evaluation of all terms in the equation for angular velocity. The properties of the Reynolds stress tensor are considered in detail because of the controlling role which it plays in the equation.

2. Vorticity equation

The mean-flow vorticity equation can be obtained by operating on the Navier–Stokes equation for mean quantities with the curl operator giving for the mean vorticity vector Ω_k the relationship

$$\rho U_j \frac{\partial \Omega_k}{\partial x_j} - \rho \Omega_j \frac{\partial U_k}{\partial x_j} = \epsilon_{ijk} \frac{\partial^2(-\rho \overline{u_l u_j})}{\partial x_i \partial x_l} + \mu \frac{\partial^2 \Omega_k}{\partial x_j \partial x_j}, \tag{1}$$

where ϵ_{ijk} is the usual alternating third-order tensor. This can also be interpreted as the equation expressing the angular momentum change for a small fluid element. The left-hand side is the product of the mass of the element and the angular acceleration following the flow and the right-hand side the sum of the moments of the forces acting on the element. Indeed, equation (1) can be derived directly by considering a small volume of fluid. The moments of the surface forces are equated to the rate of change of angular momentum of the contained fluid.

Each of the four terms in equation (1) is easily identified as a kinematic process. The first on the left-hand side represents the increase in vorticity of a fluid element by convection along a streamline. The second term represents the increase of vorticity due to stretching of the vortex lines. As such it embodies the effect of increasing angular velocity of a stream tube as it passes through a constriction. Thus the area of the stream tube must change in the flow direction for this term to be non-zero. It is evident that in uniform flow in a duct it must be zero and thus is not a factor in the flow considered herein. The terms on the right-hand side, which express the effects of the turbulent and viscous stresses respectively, tend to increase the angular momentum of a particle if directed in the same sense as the vorticity vector. Townsend (1956) defined this process as the production of vorticity. If directed in the opposite sense the effect is the destruction of vorticity.

The kinematic effect of the turbulent field on the mean flow is demonstrated by expanding the first term on the right and introducing the turbulent vorticity $\omega_k = \epsilon_{ijk}(\partial u_j/\partial x_i)$, giving a form analogous to the term on the left

$$\epsilon_{ijk} \frac{\partial^2(-\rho \overline{u_l u_j})}{\partial x_i \partial x_l} = -\left(\rho \overline{u_j \frac{\partial \omega_k}{\partial x_j}} - \rho \overline{\omega_j \frac{\partial u_k}{\partial x_j}}\right). \tag{2}$$

Thus these are respectively the increase of mean-flow angular momentum due to the average convection of turbulent vorticity and to the average stretching of turbulent vortex lines. However, without a clear physical picture of the turbulent field the sign and magnitude of the terms are not evident. On the other hand, the effect of the viscous term is well understood. This represents the diffusion

of vorticity down its gradient, tending to make vorticity evenly distributed in space.

For flow in non-circular ducts the x_1-axis is defined in the direction of the duct centreline and x_2 and x_3 are orthogonal co-ordinates in the lateral cross-section (figure 2). The main flow is described by U_1 and the secondary flows by U_2 and U_3. For uniform flow the x_1 gradients of all velocity mean properties must be zero and thus the first component of equation (1) reduces to

$$\rho U_2 \frac{\partial \Omega_1}{\partial x_2} + \rho U_3 \frac{\partial \Omega_1}{\partial x_3} = \frac{\partial^2}{\partial x_2 \partial x_3}(\rho \overline{u_3^2} - \rho \overline{u_2^2}) - \left(\frac{\partial^2}{\partial x_2^2} - \frac{\partial^2}{\partial x_3^2}\right) \rho \overline{u_2 u_3} + \mu \left(\frac{\partial^2 \Omega_1}{\partial x_2^2} + \frac{\partial^2 \Omega_1}{\partial x_3^2}\right). \tag{3}$$

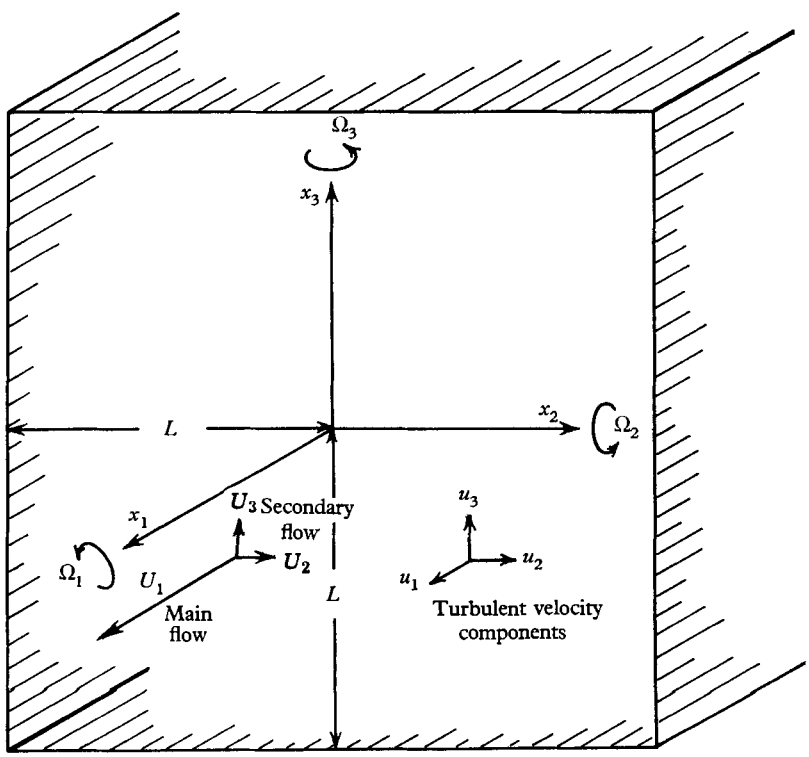

FIGURE 2. Co-ordinates for flow in a squate duct.

Because equation (3) includes only velocities and gradients in the x_2 and x_3 directions, $\Omega_1 = \partial U_3/\partial x_2 - \partial U_2/\partial x_3$ exists only if the lateral velocities exist and vice versa. The main longitudinal flow does not enter this process except as it determines the lateral turbulence components and correlations. This is even more apparent if the physical action of each term is examined. Terms on the left represent the convection of secondary vorticity by the secondary flow itself. The tendency of this process is to make the vorticity constant along the secondary flow streamlines. A similar effect is produced by the last terms on the right. These represent the diffusion of vorticity by viscosity and tend to make the vorticity uniform over the duct cross-section by diffusing it from regions of high

intensity to regions of low intensity. In a straight duct this acts to slow down the particle rotation. In laminar flow in ducts these are the only terms in the equation since Reynolds stresses do not exist. Hence, secondary flows cannot occur in a uniform flow because flow mechanisms serve only to transport and destroy vorticity. A different situation must occur in turbulent flows with the possible addition of the production terms. Thus, a steady-state condition can be obtained with the production term accelerating the fluid particle about the x_1-axis and the diffusion terms tending to decelerate the particle. Convection by the secondary flow serves to transport vorticity from regions of production to regions of diffusion. Thus, the most important term in equation (3) is the production of vorticity but the magnitude of this cannot be determined from general equations. The size and distribution of the Reynolds stresses must be considered.

3. Reynolds stress tensor for flow in a square duct

For a square cross-section the flow properties are symmetrical with respect to axes through the mid-points of the sides, x_2 and x_3, and to axes along the diagonals, $x_{2'}$, and $x_{3'}$. Thus the Reynolds stress tensor can be shown to have simplified forms along these axes. Geometrical relations are written for the velocity components related to the two systems of axes and the symmetry conditions imposed. As a result relationships are derived for the components of the tensor. At the centre of the channel, $x_2 = x_3 = 0$, and the Reynolds stress tensor consists of the three diagonal components of which two, $\overline{u_2^2}$ and $\overline{u_3^2}$ are equal. All off-diagonal components must be zero. Along the x_2-axis the tensor is invariant under a 90° rotation and may be simplified to the form

$$\rho\overline{u_i u_j} = \rho\begin{pmatrix} \overline{u_1^2} & \overline{u_1 u_2} & 0 \\ \overline{u_1 u_2} & \overline{u_2^2} & 0 \\ 0 & 0 & \overline{u_3^2} \end{pmatrix}. \tag{4}$$

For the same reason the tensor is simplified along the diagonals. The form on the $x_{3'}$-axes, which is obtained by a 45° clockwise rotation of the x_3-axis, is

$$\rho\overline{u_i u_j} = \rho\begin{pmatrix} \overline{u_1^2} & \overline{u_1 u_2} & \overline{u_1 u_2} \\ \overline{u_1 u_2} & \overline{u_2^2} & \overline{u_2 u_3} \\ \overline{u_1 u_2} & \overline{u_2 u_3} & \overline{u_2^2} \end{pmatrix}. \tag{5}$$

For a traverse taken from the x_2-axis to the $x_{3'}$-axis it is apparent that the Reynolds stress tensor must vary smoothly from its form on the x_2-axis to its form on the $x_{3'}$-axis, since discontinuities do not occur in fluid stresses.

The zones of x_1 vorticity production can be inferred from these relations. Consider the sector defined by the x_2-axis, $x_2 = L$ and the $x_{3'}$-axis. Along the x_2-axis there can be no x_3-derivative of $(\overline{u_2^2} - \overline{u_3^2})$ even though the x_2-derivative may exist since symmetry exists in the x_3-direction. The tensor component $\overline{u_2 u_3}$ must be of opposite sign on either side of the x_2-axis and is zero along the x_2-axis, that is the axis is a line of inflexion. Hence, the second derivative of $\overline{u_2 u_3}$ in the x_2-direction is zero because $\overline{u_2 u_3} = 0$ and is zero in the x_3-direction because

of the line of inflexion. Thus neither of the production terms in equation (3) is finite on the x_2-axis. The same situation is obtained for points along the $x_{3'}$-axis since the production terms transform as follows

$$\left(\frac{\partial^2}{\partial x_2^2}-\frac{\partial^2}{\partial x_3^2}\right)\overline{u_2u_3}=\frac{\partial^2}{\partial x_{2'}\partial x_{3'}}(\overline{u_{2'}^2}-\overline{u_{3'}^2}) \tag{6a}$$

$$\frac{\partial^2}{\partial x_2\partial x_3}(\overline{u_3^2}-\overline{u_2^2})=\left(\frac{\partial^2}{\partial x_{3'}^2}-\frac{\partial^2}{\partial x_{2'}^2}\right)\overline{u_{2'}u_{3'}}, \tag{6b}$$

and the arguments are identical to those above but are based on the $x_{2'}$, $x_{3'}$ co-ordinates. Along the wall the production of vorticity must be zero because the Reynolds stresses are zero at the surface and very small within the viscous sublayer. Furthermore, arguments based on symmetry with an image duct located on the other side of the wall also give this result.

Production of vorticity must therefore occur within the triangular sector, but derivations based on symmetry cannot yield information as to the areas where it will be maximum. The structure of the turbulent field must be fully understood before this can be derived and data on the required stress components is lacking. However, the large-scale properties of flow in circular ducts must be the same for all ducts. Near the centreline the intensity of turbulence and Reynolds stress tensor are influenced by the large eddies which come from all of the wall directions. The result is a turbulent field which is axi-symmetric and thus the production of vorticity must be very small. Further evidence of this pattern is the circular shape of the isovels (figure 1). Close to the wall the turbulent field is controlled by the attached eddies described by Townsend (1956). The strength of these at any location along the wall should be determined by the local wall shear. Since the secondary currents have made this uniform, the turbulent field should also be uniform. Thus, in the strip along the wall, $\overline{u_2u_3}$ should be negligible and gradients of turbulence properties in the x_3-direction very small. There must therefore be negligible production of vorticity in the region near the wall which leaves only the area near the diagonal as a possible region from which vorticity may arise. It can be shown that within this triangular sector the production must be negative, that is, tending to produce clockwise rotation of fluid elements, but experimental observation that the second of the two production terms in equation (3) is much smaller than the first is required. Considering the first term and the analogous data from a circular pipe lends to the conclusion that $\partial(\overline{u_3^2}-\overline{u_2^2})/\partial x_2$ is positive along the x_2-axis. Thus since $(\overline{u_3^2}-\overline{u_2^2})$ is zero along the diagonal and assuming a monotonic variation between the two lines, we have an indication that $\partial^2(\overline{u_3^2}-\overline{u_2^2})/(\partial x_2\partial x_3)$ is negative in the region of production. This is consistent with Prandtl's contention that the flow is into the corners.

In conclusion it is noted that there are eight possible subsections of the square channel which satisfy the conditions of symmetry, each of which is identical in shape to the one examined. Symmetry also dictates that each contains a secondary current with an independent production, diffusion and convection of x_1 vorticity. The conditions of symmetry about the x_2- and x_3-axes further imply that the production of vorticity will be opposite in sense in adjacent subsections,

since $\overline{u_2 u_3}$ changes sign at the x_2- and x_3-axes and $(\overline{u_3^2} - \overline{u_2^2})$ changes sign at the x_2- and x_3-axes. Thus there must be four positive and four negative circulations grouped as opposing pairs with one pair at each corner of the duct.

4. Experimental equipment and techniques

Experimental data was obtained from a 3 in. square, 70 ft. long horizontal duct made of plastic-coated plywood. A calibrated flow nozzle and fan supplied air at room temperature. In a previous investigation with this equipment Leutheusser (1963) confirmed that the flow was uniform at the plane of measurement, near the exit, and proceeded to determine the longitudinal velocity components.

The present investigation provided quantitative data for the secondary currents and Reynolds stress tensor by utilizing a constant-current hot-wire anemometer. The hot-wire filaments were 0·0003 in. tungsten wires with an active length of 0·040 in. The hot-wire was held by a traversing gear which could be positioned to $\pm$ 0·0001 in. The anemometer circuit consisted of the standard Flow Corporation HWB 2 bridge with frequency compensation, and the Flow Corporation random signal voltmeter 12 A 1. The secondary-current data were obtained by using a standard HWP-B probe and the sensitive galvanometer balance circuit of the HWB 2 bridge. The traversing gear for this experiment positioned the wire to $\pm$ 0·0001 in. as well as rotating the wire to $\pm$ 1/10 degree.

Measurements of secondary currents

The sensitivity of a hot-wire to flow direction permits measurements of flow direction to be made, particularly when the filament is operated at a high temperature and at large angles of incidence. For determination of the U_2 component a HWP-B probe was mounted with the probe axis in the x_3-direction. At the centreline of the channel a rotational protractor was calibrated. The probe was rotated until the wire was at a rotational angle, β^+, of 60° with respect to the position when flow is normal to the wire. In the β^+ position the Wheatstone bridge was balanced for a wire resistance ratio of 1·4 by using a stable current supply. The probe was then rotated in the negative direction until the bridge again balanced giving the β^- position at the centre line to within 1/10 degree by means of a vernier. The calibrated positions were then used as a basis for the subsequent readings. The procedure used at the centreline was repeated throughout the flow with variations in β^- indicating the yaw of the approaching flow and the magnitude of the U_2 component which was determined from

$$\frac{U_2}{U_1} = \tan\left(\frac{\bar{\beta}_{C\text{-}L} - \bar{\beta}^-}{2}\right). \tag{7}$$

Positioning the probe in the x_2-direction, the U_3 velocity was similarly obtained. With the three components of U_i thus measured flow directions could readily be determined.

Measurement of the Reynolds stress tensor

The present investigation employed a method of determining all components of the Reynolds stress tensor which was devised to produce the maximum experimental accuracy. The component was first evaluated by mounting a standard

probe with the hot-wire normal to the direction of flow. Next, the lateral velocity fluctuations were measured by a probe with a hot-wire inclined to the direction of flow. The particular probe was mounted in the x_1-direction with a wire inclined at an angle of $\beta = 41{\cdot}5°$. The angle of the wire was accurately determined by an optical comparator. Considering the recent evaluations by Hinze (1959) and Webster (1962) the sensitivity of a hot-wire to the angle of incidence is

$$(\text{sensitivity})_\beta^2 = (\text{sensitivity})_{\beta=0}^2(\cos^2\beta + A^2\sin^2\beta), \tag{8}$$

where A is a constant characteristic of the probe. For this particular probe A was experimentally determined to be 0·333. Thus the ratio of the longitudinal and lateral sensitivities S_1 and S_2 for this wire is

$$\frac{S_1^2}{S_2^2} = \frac{\sin^2 41{\cdot}5° + 0{\cdot}10\cos^2 41{\cdot}5°}{\cos^2 41{\cdot}5° + 0{\cdot}10\sin^2 41{\cdot}5°} = 0{\cdot}823. \tag{9}$$

It is worth noting that a 9·1 % error in the lateral sensitivity would have arisen if the hot-wire had been assumed to be at the design value of 45°. As the probe is rotated about its shaft the ratio of sensitivities is unaffected provided that the mean flow is parallel to the shaft. When the hot-wire is in the (x_1, x_2)-plane the x_1- and x_2-components of the instantaneous velocity are measured in the combination

$$e_{12} = C(S_1 u_1 + S_2 u_2), \tag{10}$$

where C is the amplifier calibration which is normally constant during an experiment. Squaring the signal and taking the time average gives

$$\overline{e_{12}^2} = C^2S_1^2[\overline{u_1^2} + 1{\cdot}82\overline{u_1u_2} + 0{\cdot}823\overline{u_2^2}]. \tag{11a}$$

As the probe is rotated by 45° increments there results

$$\overline{e_{13'}^2} = C^2S_1^2[\overline{u_1^2} + 1{\cdot}82\,\overline{u_1u_{3'}} + 0{\cdot}823\overline{u_{3'}^2}], \tag{11b}$$

$$\overline{e_{13}^2} = C^2S_1^2[\overline{u_1^2} + 1{\cdot}82\overline{u_1u_3} + 0{\cdot}823\overline{u_3^2}], \tag{11c}$$

$$\overline{e_{1-2'}^2} = C^2S_1^2[\overline{u_1^2} - 1{\cdot}82\overline{u_1u_{2'}} + 0{\cdot}823\overline{u_{2'}^2}], \tag{11d}$$

$$\overline{e_{1-2}^2} = C^2S_1^2[\overline{u_1^2} - 1{\cdot}82\overline{u_1u_2} + 0{\cdot}823\overline{u_2^2}], \tag{11e}$$

$$\overline{e_{1-3'}^2} = C^2S_1^2[\overline{u_1^2} - 1{\cdot}82\overline{u_1u_{3'}} + 0{\cdot}823\overline{u_{3'}^2}], \tag{11f}$$

$$\overline{e_{1-3}^2} = C^2S_1^2[\overline{u_1^2} - 1{\cdot}82\overline{u_1u_3} + 0{\cdot}823\overline{U_3^2}], \tag{11g}$$

$$\overline{e_{12'}^2} = C^2S_1^2[\overline{u_1^2} + 1{\cdot}82\overline{u_1u_{2'}} + 0{\cdot}823\overline{u_{2'}^2}]. \tag{11h}$$

Combination of these eight readings gives most of the components directly. For example, $\overline{u_1u_2}$ is obtained by subtracting $\overline{e_{1-2}^2}$ from $\overline{e_{12}^2}$, and similarly $\overline{u_1u_3}$ is determined. The terms required for the production of vorticity are obtained by taking the sum of equations (11*a*) and (11*e*) and subtracting (11*c*) and (11*g*) which gives $(\overline{u_2^2} - \overline{u_3^2})$ and taking the sum of equations (11*d*) and (11*h*) and subtracting (11*b*) and (11*f*) which gives $\overline{u_{2'}^2} - \overline{u_{3'}^2} = -2\overline{u_2u_3}$. Thus these are all obtained using the same wire under identical operating conditions giving maximum

Position x_2	Position x_3	$\frac{\overline{u_1u_1}}{U_\tau^2}$	$\frac{\overline{u_2u_2}}{U_\tau^2}$	$\frac{\overline{u_3u_3}}{U_\tau^2}$	$\frac{\overline{u_1u_2}}{U_\tau^2}$	$\frac{\overline{u_1u_3}}{U_\tau^2}$	$\frac{\overline{u_2u_3}}{U_\tau^2}$	$\frac{(\overline{u_2u_2}-\overline{u_3u_3})}{U_\tau^2}$	$\frac{\overline{U_1}}{U_{C\text{-}L}}$	$\frac{U_{sec}}{U_\tau}$	Orientation angle θ ($\theta = 0$ for pos. x_2 direction)
Centre-line at (1·5 in. × 1·5 in.)											
1·5	1·5	1·11	1·808	0·808	0	0	0	0	1·000	0	0
1·3	—	1·34	0·845	0·953	0·357	0	0	−0·099	0·988	0	0
1·1	—	1·86	1·11	1·14	0·708	0	0	−0·093	0·970	0	0
0·9	—	2·46	1·20	1·39	0·927	0	0	−0·185	0·945	0·021	180
0·7	—	3·24	1·34	1·82	1·06	0	0	−0·490	0·905	0·103	180
0·5	—	4·02	1·47	2·11	1·21	0	0	−0·642	0·860	0·271	180
0·3	—	5·01	1·50	2·38	1·38	0	0	−0·887	0·798	0·162	180
0·1	1·5	6·10	1·54	2·60	1·60	0	0	−1·06	0·700	0·142	180
1·3	1·3	1·36	1·11	1·11	0·278	+0·271	−0·079	0	0·984	0·217	45
1·1	—	1·75	1·08	1·14	0·576	+0·112	−0·099	−0·053	0·970	0·242	63·1
0·9	—	2·38	1·20	1·40	0·861	0	−0·086	−0·199	0·943	0·235	63·1
0·7	—	3·15	1·28	1·79	1·03	−0·060	−0·040	−0·503	0·911	0·240	110
0·5	—	4·02	1·46	1·86	1·19	−0·060	0	−0·397	0·860	0·139	114
0·3	—	5·01	1·51	2·34	1·36	−0·066	0	−0·834	0·800	0·322	243·5
0·1	1·3	6·10	1·54	2·60	1·60	−0·060	0	−1·06	0·700	0·258	255
1·1	1·1	1·62	1·16	1·16	0·344	+0·344	−0·086	0	0·964	0·214	45
0·9	—	2·15	1·20	1·64	0·688	+0·112	−0·079	−0·172	0·947	0·248	59·1
0·7	—	2·89	1·25	1·66	0·907	−0·093	−0·066	−0·404	0·917	0·160	48·2
0·5	—	3·83	1·40	1·97	1·14	−0·139	−0·053	−0·563	0·870	0	0
0·3	—	4·90	1·51	2·22	1·35	−0·139	−0·040	−0·715	0·813	0·183	270
0·1	1·1	6·10	1·54	2·60	1·58	−0·093	0	−1·06	0·719	0·284	270
0·9	0·9	1·93	1·26	1·26	0·344	+0·344	−0·079	0	0·965	0·248	45
0·7	—	2·38	1·20	1·46	0·688	+0·060	−0·086	−0·258	0·919	0·322	50·2
0·5	—	3·53	1·26	1·79	1·01	−0·159	−0·079	−0·523	0·883	0·175	333·5
0·3	—	4·73	1·51	2·08	1·29	−0·159	−0·040	−0·569	0·827	0·237	308·8
0·1	0·9	5·97	1·54	2·58	1·55	−0·093	0	−0·106	0·719	0·284	270
0·7	0·7	2·04	1·26	1·26	0·344	+0·344	−0·172	0	0·915	0·405	45
0·5	—	2·79	1·20	1·50	0·735	−0·112	−0·132	−0·298	0·892	0·250	331·5
0·3	—	4·29	1·40	1·89	1·21	−0·079	−0·066	−0·490	0·837	0·209	333·1
0·1	0·7	5·85	1·54	2·46	1·52	−0·093	−0·020	−0·927	0·719	0·335	270
0·5	0·5	2·30	1·34	1·34	0·344	+0·344	−0·205	0	0·878	0·379	45
0·3	—	3·72	1·31	1·66	1·01	+0·066	−0·093	−0·344	0·829	0·359	8·9
0·1	0·5	5·24	1·52	2·45	1·49	0	−0·053	−0·927	0·709	0·361	290
0·3	0·3	2·79	1·43	1·43	0·344	+0·344	−0·192	0	0·800	0·258	45
0·1	0·3	4·34	1·52	2·38	1·38	+0·112	−0·046	−0·861	0·691	0·206	306
0·1	0·1	3·57	2·00	2·00	0·344	+0·344	−0·046	0	0·628	0·194	45

$U_{C\text{-}L}$ = 65·9 ft./sec, U_{av} = 54·8 ft./sec, U_τ = 2·55 ft./sec.

TABLE 1. Mean-velocity and turbulent-velocity correlations for a 3 in. × 3 in. square channel for Reynolds number of 83,000

accuracy. The variation and inaccuracy of determination of C and S_1 leads to considerable scatter of results taken from different wires. This, however, is required if $\overline{u_2^2}$ or $\overline{u_3^2}$ are determined. Hence these components were not determined as accurately as the difference between them.

5. Experimental results

All of the terms in the x_1-vorticity equation were measured for the square duct for the triangular sector described above. Some mean flow characteristics were also measured to provide a general description of the flow. All results were

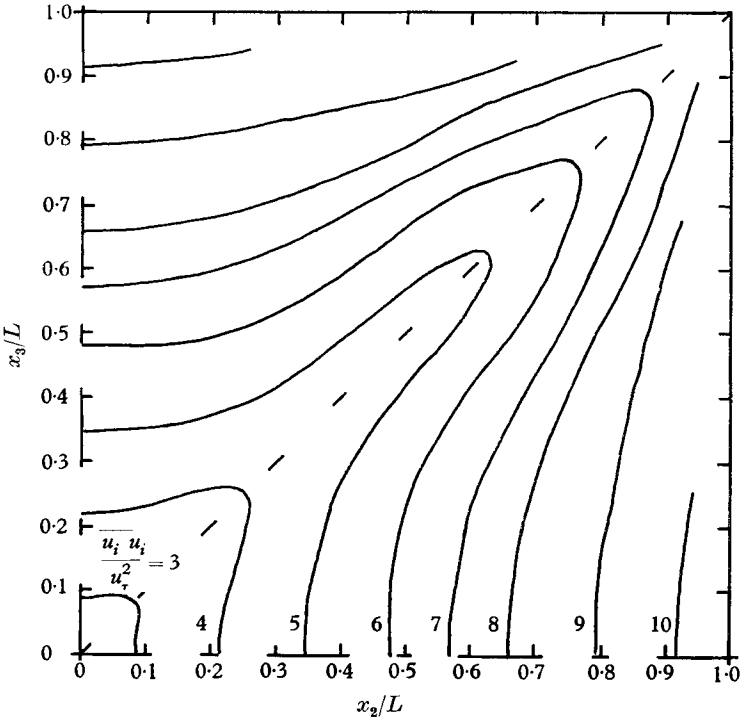

FIGURE 3. Lines of constant turbulence kinetic energy for flow in a square duct, U_q = 65·9 ft./sec, U_τ = 2·55 ft./sec, $U_{av}D_e/\nu$ = 83,000.

made dimensionless using the characteristic length L and velocity U_τ, the average shear velocity, with the exception of the U_1 velocity components which Leutheusser (1963) made dimensionless by using the duct centreline velocity $U_{C\text{-}L}$. Table 1 contains data of the longitudinal velocity components, secondary velocity components, and all the components of the Reynolds stress tensor for the 3 in. by 3 in. duct. Figure 1 shows the isovel pattern for the mean velocity as determined by Leutheusser (1963). The distortion of the isolvels in the corner regions is clearly evident. Figure 3 is a plot of the turbulence energy in the duct, which is lowest at the centre and highest in the wall region where turbulence is produced. It is evident that the turbulence field is more distorted by the secondary flow than is the mean velocity field.

The secondary current pattern plotted in figure 4 confirms the pattern predicted by Prandtl, and is smaller in magnitude than the turbulent velocities from which it originates. The x_1-vorticity field is shown in figure 5 and was obtained by Hoagland (1960) from the secondary current data. This was confirmed independently in the present investigation. The convection of x_1-vorticity was

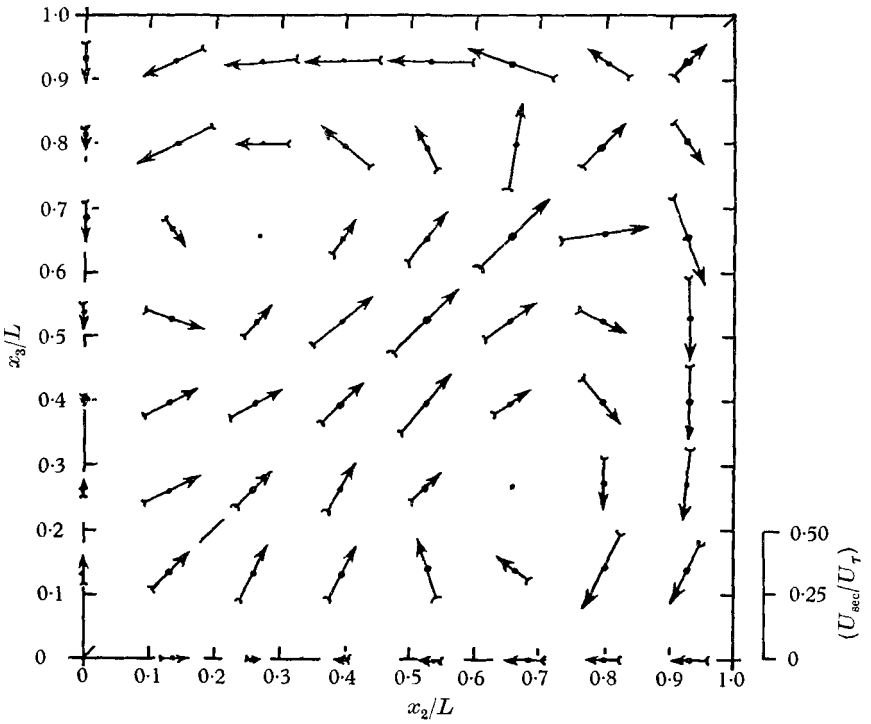

FIGURE 4. Secondary flow in a square duct, $U_{C\cdot L} = 65{\cdot}9$ ft./sec, $U_\tau = 2{\cdot}55$ ft./sec, $U_{av}D_e/\nu = 83{,}000$.

obtained from tabulated and faired data of the secondary currents and x_1-vorticity by a finite-difference technique. Higher accuracy was obtained by using the equivalent vectorial form

$$U_j \frac{\partial \Omega_1}{\partial x_j} = |U_{\text{secondary}}|\,|\nabla \Omega_1| \cos \alpha,$$

where α is the angle between the secondary current and vorticity gradient vectors. The resulting data are plotted in figure 6. The finite-difference method of determining the first and second derivatives is of the same order of magnitude as the error in the function. This is true if the spatial resolution is known to a high accuracy as is the case with the above-mentioned traversing gear. Similarly Kunz (1957) shows that the error of the second derivative is only twice the error of the original function.

The turbulence correlations associated with vorticity production are plotted in figures 7 and 8. The magnitude of the production of x_1-vorticity was obtained from these correlations by a finite-difference technique. In the analysis the

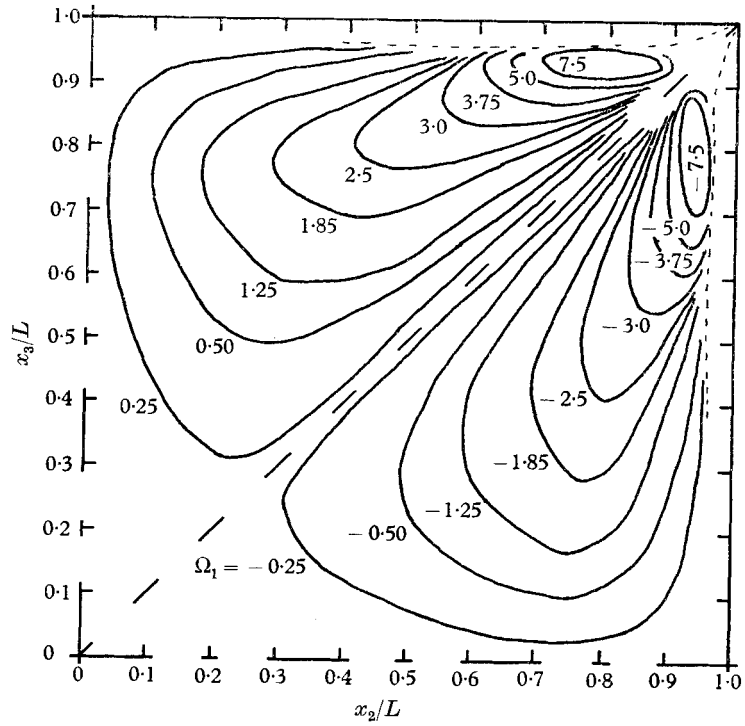

FIGURE 5. Lines of constant vorticity Ω (dimensionless) for flow in a square duct, $L = 2{\cdot}5$ in., $U_{C\text{-}L} = 28{\cdot}5$ ft./sec, $U_{av} = 22{\cdot}9$ ft./sec, $U_{av}D_e/\nu = 60{,}000$ (Hoagland 1960).

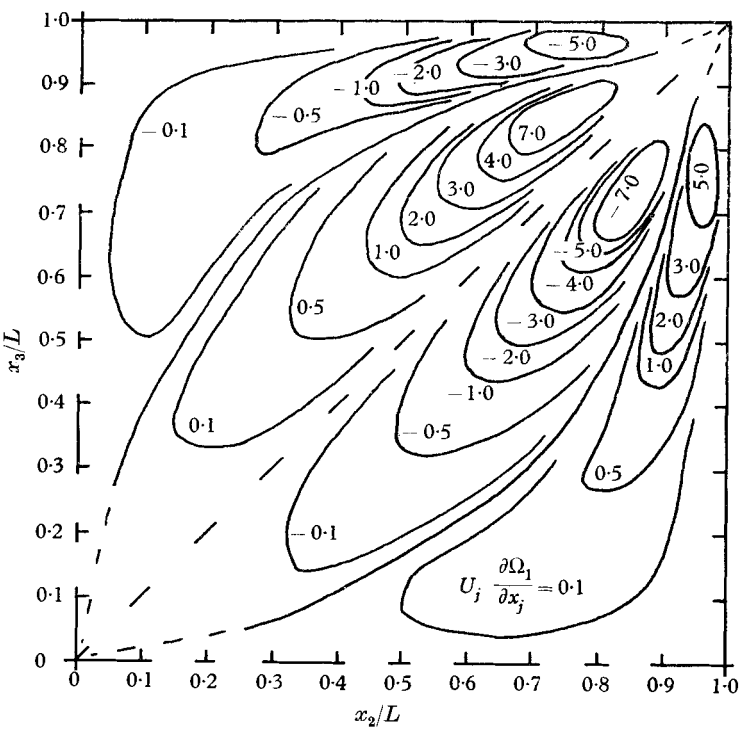

FIGURE 6. Convection of vorticity (dimensionless) for flow in a square duct, $U_{av}D_e/\nu = 83{,}000$.

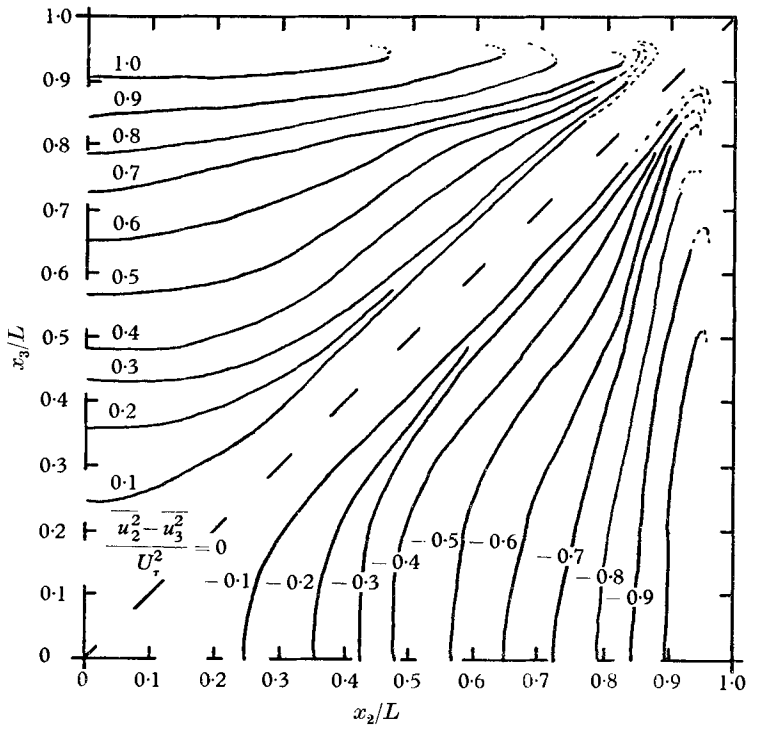

FIGURE 7. Turbulence correlation $(\overline{u_2^2}-\overline{u_3^2})/U_\tau^2$ for flow in a square duct, $U_{av}D_e/\nu = 83{,}000$.

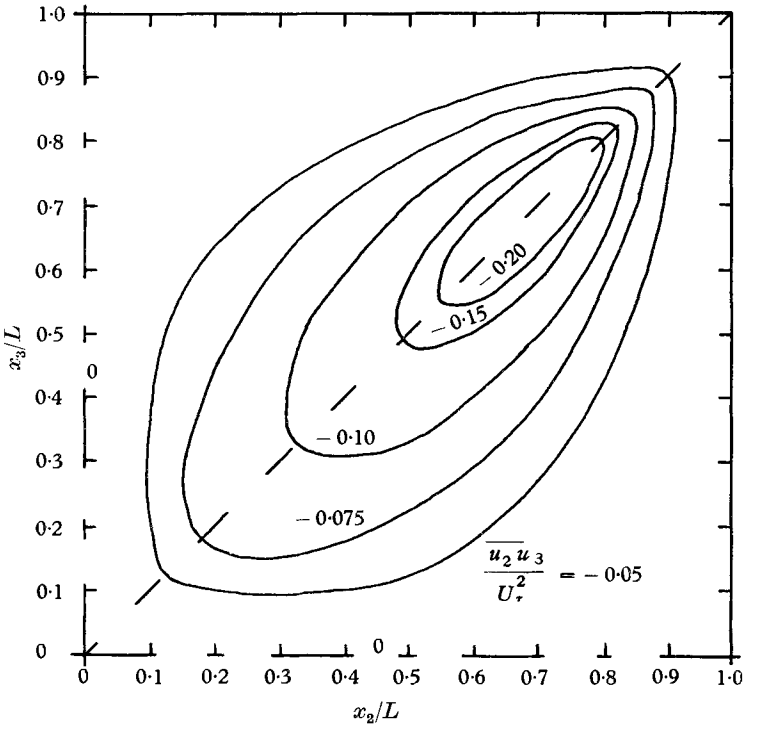

FIGURE 8. Turbulence correlation $\overline{u_2 u_3}/U_\tau^2$ for flow in a square duct, $U_{av}D_e/\nu = 83{,}000$.

contribution of $\overline{u_2 u_3}/U_\tau^2$ was found to be negligible, the correlation is an order of magnitude smaller than $(\overline{u_2^2}-\overline{u_3^2})/U_\tau^2$, and furthermore the second-order derivatives tended to be self-cancelling. Thus the production x_1-vorticity was accurately described by the first term *in equation (3)*. As seen in figure 9 the region of maximum production lies near the x_3-axis and is distant from the wall and hence is removed from the region correlated by the inner law. The production is negative, wherever it exists, indicating that there is a similar flow mechanism everywhere in the sector, Reynolds stresses acting only to produce clockwise rotations.

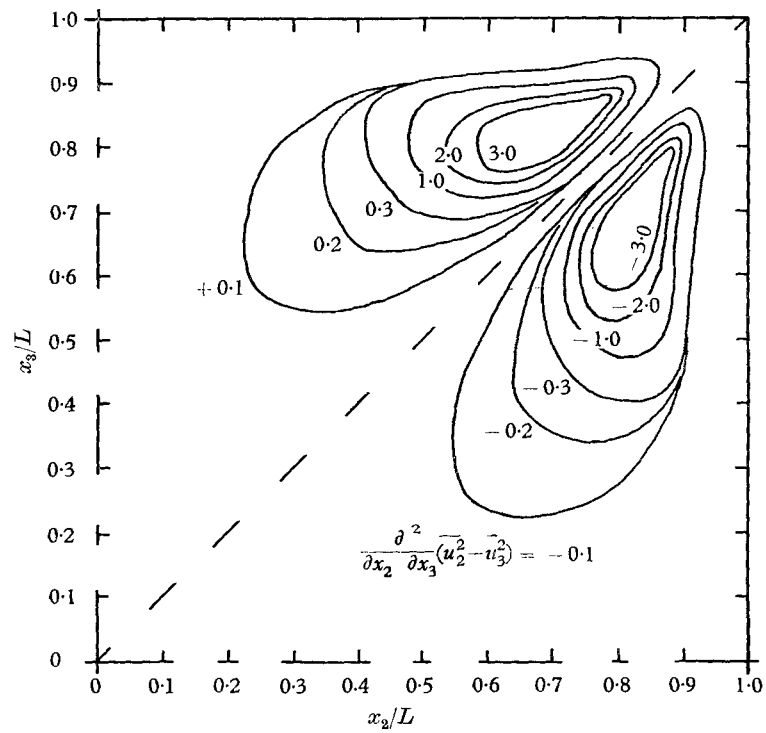

FIGURE 9. Production of vorticity (dimensionless) for flow in a square duct, $U_{av}D_e/\nu = 83{,}000$.

The diffusion of vorticity was obtained from tabulations of the x_1-vorticity shown on figure 5 by finite difference methods, and is plotted in figure 10. The diffusion of vorticity is most intense near the wall and towards the corner. It is obviously associated with the viscous stresses which are largest in the neighbourhood of the corner. Since the region of diffusion occurs nearer the wall than the region of production, the convection of vorticity must be from the region of production to the region of diffusion as shown in figure 6.

As can be seen from figures 7, 10 and 11, the balancing of the vorticity equation is good at all points in the cross-section. Zones of vorticity production are balanced by vorticity convection away from these zones. Similarly, vorticity diffusion is balanced by vorticity convections to these regions.

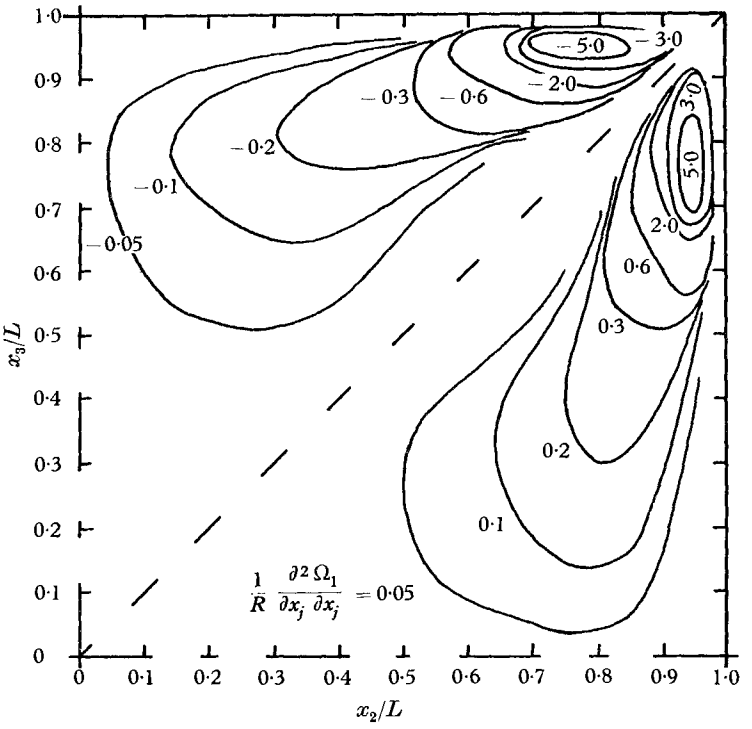

FIGURE 10. Diffusion of vorticity (dimensionless) for flow in a square duct, $U_{av}D_e/\nu = 83{,}000$.

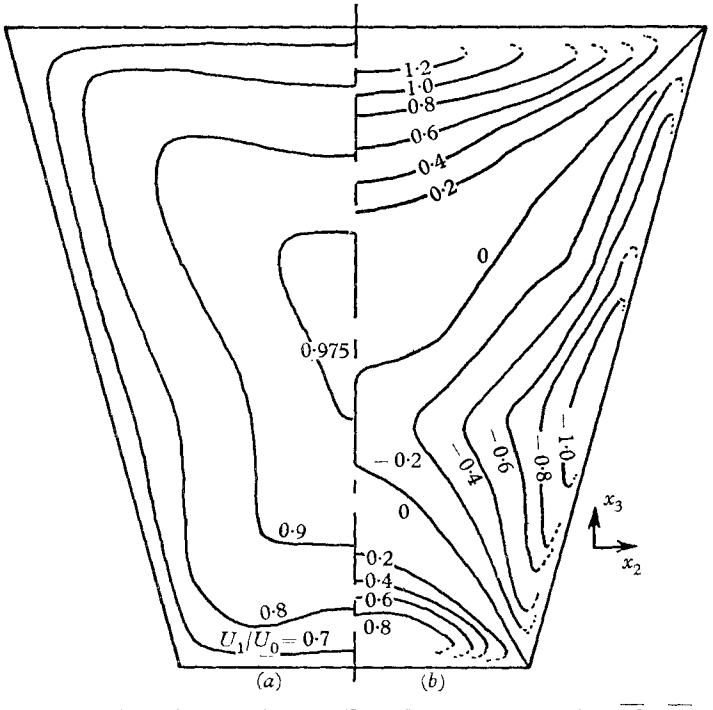

FIGURE 11. Isovels of (*a*) axial velocity and (*b*) turbulence correlation $(\overline{u_2^2}-\overline{u_3^2})/U_\tau^2$ for flow in a trapezoidal duct, height = 18·3 cm, $U_{C\text{-}L} = 83{\cdot}1$ ft./sec, $U_{av} = 68{\cdot}9$ ft./sec, $U_\tau = 3{\cdot}01$ ft./sec, $U_{av}D_e/\nu = 240{,}000$ (Rodet 1960).

6. Effect of Reynolds number

The vorticity equation presented in §2 is in dimensional form, thus the data obtained for different test conditions cannot be directly related. To overcome this difficulty equation (3) can be placed in dimensionless form by dividing lengths by the half width of the duct L and velocities by the average shear velocity. Any other velocity could be chosen on dimensional grounds alone but the shear velocity is physically the most significant since the secondary flows are akin to the velocity defect used in formulating the outer laws of Townsend (1956). Thus the production and convection terms can be expressed in dimensionless variables only, that is

$$U_j \frac{\partial \Omega_1}{\partial x_j} - \Omega_j \frac{\partial U_1}{\partial x_j} = \overline{u_j \frac{\partial \omega_1}{\partial x_j}} - \overline{\omega_j \frac{\partial u_1}{\partial x_j}} + \frac{\nu}{U_\tau L} \frac{\partial^2 \Omega_1}{\partial x_j \partial x_j}. \tag{12}$$

All dimensional factors are embodied in the multiplication of the diffusion term. The ratio $U_\tau L/\nu$ is a cross-section Reynolds number.

There is some justification for assuming that the first four terms are independent of the Reynolds number. In all flows at large Reynolds number those properties not associated with the dissipation of energy are found to be similar for variations of the Reynolds number, cf. Townsend (1957). Thus, considering the physical processes involved, convection of vorticity is based on the mean flow, and production arises due to the action of the largest eddies. If equation (12) is to balance for all Reynolds numbers, the vorticity diffusion term must be constant as well. This can only result in the second-order derivatives of Ω_1 varying inversely with the Reynolds number.

The experimental data available from all sources appears to bear out this behaviour. The secondary currents in a square channel appear to be independent of the Reynolds number in the regions not close to the corner, since no variations in strength or orientation can be detected in the range of Reynolds numbers from 20,000 to 83,000 based on the average velocity U_{av}. The convection of vorticity is thus independent of Reynolds number and the same result is seen in the data for vorticity production. Diffusion was found to be significant only in the wall region which is correlated by the inner law, and thus must depend on the Reynolds number. As noted above, it must also vary inversely with the Reynolds number at any given point. Thus the effect of Reynolds number on the secondary current streamlines can be predicted.

Consider first the region very close to the wall where the streamlines are parallel to the wall, so that

$$\Omega_1 = \partial U_3/\partial x_2,$$

and the diffusion of vorticity simplifies to

$$\frac{\nu}{U_\tau L} \frac{\partial^2 \Omega_1}{\partial x_j \partial x_j} = \frac{1}{R} \frac{\partial^3 U_3}{\partial x_2^3}.$$

For this term to be constant the secondary currents must extend closer to the wall as the Reynolds number increases. Applying this type of analysis to the area close to the corner leads to the conclusion that the secondary currents may also penetrate further into the corners as the Reynolds number increases. It is

seen that very small adjustments to the patterns are sufficient to alter the third derivatives significantly and that these required changes could not be measured with the techniques used in this study. However, the wall shear measurements of Leutheusser (1963) do indicate an increasing corner penetration and an increasing averaging of the wall shear velocity as the Reynolds number increases. It appears that the approach of the secondary currents to the wall is a similar phenomenon to the decreasing thickness of the viscous sublayer with increasing Reynolds numbers.

In summary, the secondary currents must approach the walls as the Reynolds number increases. The resulting constancy of the dimensionless vorticity diffusion makes the diffusion compatible with the production and convection of vorticity, which are independent of the Reynolds number.

7. Vorticity in ducts of other shapes

The development presented in the preceding sections for the square duct could be repeated for any regular polygon cross-section. The basic tenets were the required symmetry of the Reynolds stress tensor about the lines connecting the centre to the mid-points of the sides and to the corners. Geometry alone requires that there be twice as many sectors as sides and that the circulation be of opposite sense in adjoining sectors. From experimental measurements it is apparent that the sign of vorticity is such as to produce secondary flows towards the corners with the production of vorticity occurring in the zone defined by the corner bisector and wall. The conditions of corner symmetry can be extended to any polygon with the requirement that the number of sectors must be twice the number of sides. Since polygons with a large number of sides must approach the flow properties of a circular section, it is certain that as the number of sides is increased the longitudinal vortices must be smaller in magnitude and more concentrated in the neighbourhood of the corners. Thus there must be a critical Reynolds number for each polygon below which Ω_1 is zero everywhere since the zone of production will be within the inner law flow régime, a régime which does not appear to be associated with vorticity production.

Rodet (1960) studied the structure of turbulence in a trapezoidal duct with corner angles of 75° and 105°, a shape which is a small distortion of a square. His results which form the bases of figure 11 show that the isovels are roughly symmetrical with respect to the corner bisectors. The plot of $(\overline{u_2^2}-\overline{u_3^2})$ is also nearly symmetrical about the corner bisectors. Unfortunately this data is in error since the turbulence measurements were made parallel and normal to the top. If all of the Reynolds stress tensor components had been measured the tensor could have been rotated to the co-ordinate set $x_1 x_2' x_3'$ which would be symmetrical about the bisector. It is believed that the resulting turbulence correlation $(\overline{u_2'^2}-\overline{u_3'^2})$ would display the required corner symmetry. Nevertheless, it does appear from inspection of figures 7 and 11 that the region of greatest vorticity production is near the corner bisectors in square and trapezoidal ducts. In more general terms the production should be thus associated with a line perpendicular to the boundary at its point of maximum curvature for any general duct contour.

Considerably more information is available on flow in a duct with a 3×1 rectangular section. Again the evidence points to a division of the secondary flow by the corner bisector. The four sections of figure 12 illustrate this effect but most particularly the change in sign of Ω_1. Exactly as in the case of the square

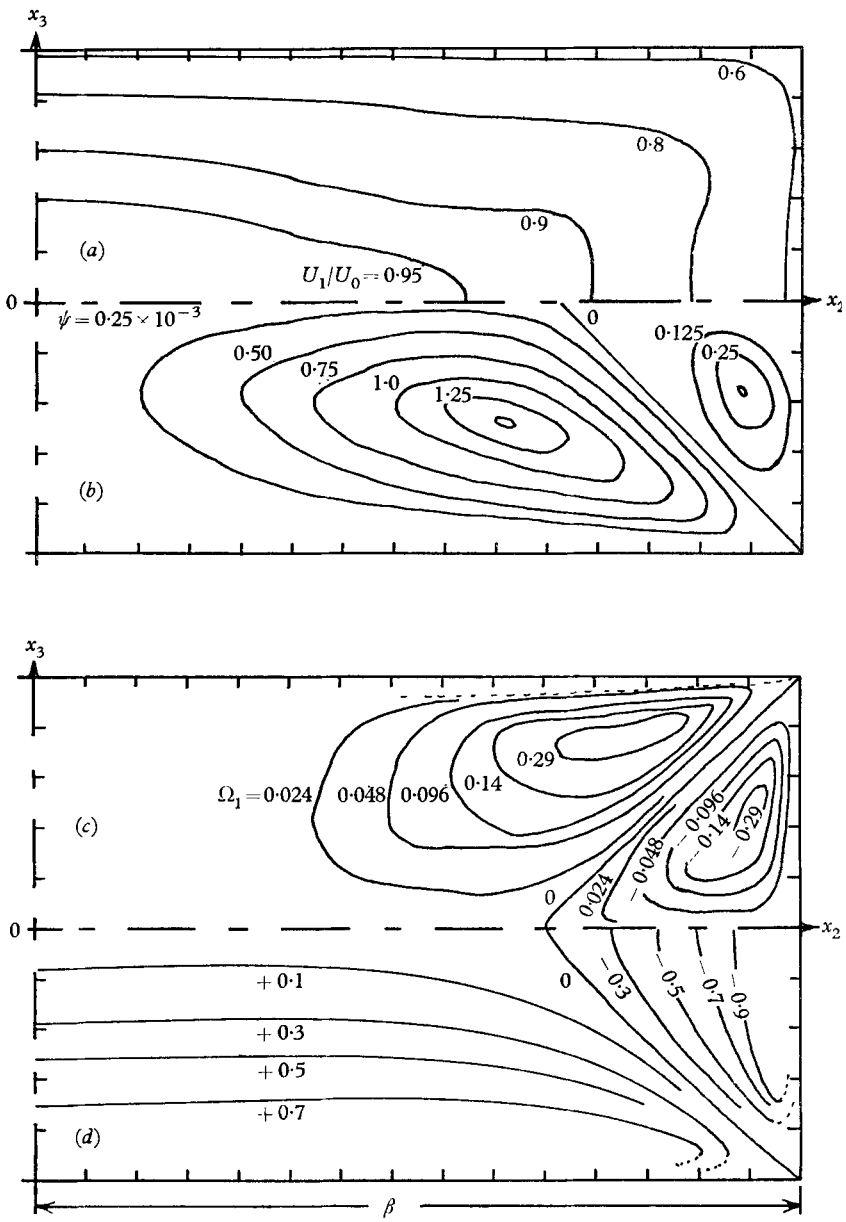

FIGURE 12. Flow in a 3 in. × 1 in. rectangular duct. (*a*) Isovels of axial velocity (Leutheusser 1963): $U_{C\text{-}L} = 29{\cdot}8$ ft./sec, $B = 1{\cdot}5$ in., $U_{av}D_e/\nu = 56{,}000$. (*b*) Secondary flow streamlines (Hoagland 1960): $U_{C\text{-}L} = 51{\cdot}8$ ft./sec, $B = 2{\cdot}5$ in., $U_{av}D_e/\nu = 60{,}000$, $B(\partial\psi/\partial x_2) = U_{secondary}/U_{C\text{-}L}$. (*c*) Lines of constant vorticity Ω_1 (dimensionless) (Hoagland 1960): $U_{C\text{-}L} = 51{\cdot}8$ ft./sec, $B = 2{\cdot}5$ in., $U_{av}D_e/\nu = 60{,}000$. (*d*) Lines of constant $(\overline{u_2^2} - \overline{u_3^2})/U_\tau^2$, $U_{C\text{-}L} = 31{\cdot}9$ ft./sec, $B = 0{\cdot}5$ in., $U_{av}D_e/\nu = 20{,}000$.

duct the sign of $(\overline{u_2^2} - \overline{u_3^2})$ changes as this bisector is reached. Within the triangular area next to the short wall the magnitude of Ω_1 and the production and diffusion of vorticity are close to the values measured in the square duct. This is consistent with the fact that the secondary flow in this zone is identical in shape to that in a square duct. Within the trapezoidal area adjacent to the long wall, a different flow pattern exists. Circulation is in the same direction everywhere but of a greater strength than in the smaller sector. There is no evidence that production is greater so it must be concluded that the vorticity second-order gradients associated with diffusion are smaller in the trapezoidal section. This is consistent with the displacement of the point of maximum Ω_1 further from the corner in the trapezoidal sector. A close examination of the isovel pattern shows that the secondary flow is not correlated everywhere to the curvature variations of the isovels. Prandtl assumed that all curvature reversals are associated with a flow circuit. For the trapezoidal sector this criterion would require two circuits, whereas Hoagland (1960) only detected one close to the corner bisector. The existence of a second vorticity is not excluded, however, since the magnitude of the circulation would be so small as to be undetected by even a hot-wire yaw meter.

In conclusion there is strong evidence to indicate that corner symmetry applies to all polygons such that the turbulence correlation $(\overline{u_2^2} - \overline{u_3^2})$ which is responsible for vorticity production is zero on the corner bisector. As a consequence, each corner of a polygon will have two circulations which are separated by the corner bisector and which direct fluid into the corner and therefore are of opposite rotation.

8. Discussion

The experimental evidence obtained from flows in square, trapezoidal and rectangular ducts enables a definitive description to be made of the secondary flows and the region where the vorticity Ω_1 is created and destroyed. However, the information is lacking which will enable the mechanism of production to be defined. Further studies of the turbulent field will need to be made before the eddy structure which produces the Reynolds stress gradients can be predicted. When an analytical description is obtained, even though it is approximate, then equation (3) can be solved to give the distribution of Ω_1 as well as the distribution and strength of the secondary flows.

Probably the most important conclusion reached from this investigation is that the production of vorticity is associated with the relative proximity of an element of fluid to the walls of the duct. In a section of a polygon this can be specifically stated as the nearest to a corner bisector. There is strong evidence that the production is always zero on a bisector and is of opposite sense on either side. Therefore a corner bisector separates a pair of independent secondary circulations. This fact can lead to pronounced simplifications in future analyses of the effects of secondary flows. This dependence of Ω_1 on the existence of a corner would preclude the possibility of secondary currents for flows between infinitely wide flat plates. Thus the usual assumption of neglecting secondary flow effects in very wide rectangular ducts is justified except in the corner regions.

There still remains the problem of relating Ω_1 and the secondary flow to distortions of the main flow. This relationship cannot be obtained from a study of the x_1-vorticity equation because the main flow does not enter directly. Thus the mean flow momentum and energy equations must be investigated. However, a complete explanation is unlikely until the simpler flow régime in pipes is fully understood.

Finally, it appears that the relationship used by Prandtl (1927) and Nikuradse (1926) to predict the nature of secondary circulations from the isovel pattern may not be correct in all cases. This conclusion is a consequence of the data for 3 in. × 1 in. rectangular channels where a double circulation in the trapezoidal section is suggested by the curvature of the isovels, while only one circulation near the corner was experimentally observed by Hoagland (1960).

In conclusion, the authors have not attempted to include tabulations of all the experimental data which were employed in the analyses; however these data can be obtained from the Ph.D. thesis of Brundrett (1963).

The authors are indebted to the Department of Mechanical Engineering of the University of Toronto and to the National Research Council of Canada for research grants which supported this experimental study.

REFERENCES

BRUNDRETT, E. 1963 The production and diffusion of vorticity in channel flow. TP 6302, Department of Mechanical Engineering, University of Toronto.

HINZE, J. O. 1959 *Turbulence, An Introduction to its Mechanism and Theory.* New York: McGraw-Hill Book Company Inc.

HOAGLAND, L. C. 1960 Fully developed turbulent flow in straight rectangular ducts... secondary flow, its cause and effect on the primary flow. Ph.D. Thesis, Department of Mechanical Engineering, Massachusetts Institute of Technology.

KUNZ, K. S. 1957 *Numerical Analysis.* New York: McGraw-Hill Book Company Inc.

LEUTHEUSSER, H. J. 1963 Turbulent flow in rectangular ducts. *Amer. Soc. of Civil Engs., J. of the Hydraulics Division,* **89**, HY 3.

NIKURADSE, J. 1926 Untersuchungen über die Geschwindigteitsverteilung in turbulenten Strömungen. Thesis, Göttingen, 1926. *V.D.I.-Forsch.* **281**.

PRANDTL, L. 1927 Über den Reibungswiderstand strömenderluft. *Ergeb. Aerodyn. Versuch., Göttingen,* III series.

RODET, E. 1960 Etude de l'écoulement d'un fluide dans un tunnel prismatique de section trapézoidale. *Publications Scientifiques et Téchniques du Ministère de L'Air,* no. 369.

TOWNSEND, A. A. 1956 *The Structure of Turbulent Shear Flow.* Cambridge University Press.

WEBSTER, C. A. G. 1962 A note on the sensitivity to yaw of a hot-wire anemometer. *J. Fluid Mech.* **13**, 307.